INTERNATIONAL JOURNAL OF FLUID POWER
2018, VOL. 19, NO. 2, 91–105
https://doi.org/10.1080/14399776.2018.1447065

Taylor & Francis
Taylor & Francis Group

A hydraulic hybrid excavator based on multi-chamber cylinders and secondary control – design and experimental validation

Kim Heybroek[a] and Mika Sahlman[b]

[a]Volvo Construction Equipment, Eskilstuna, Sweden; [b]Norrhydro OY, Tampere, Finland

ABSTRACT

In this paper, a special type of multi-chamber cylinders along with secondary controlled hydraulic motors are key components in the design of a highly efficient hydraulic series hybrid system. The system is developed for and tested on a large excavator (30-ton class). The evaluated system supports potential and kinetic energy recovery and storage using hydraulic accumulators. Through proper sizing of components and sophisticated valve control, an energy-efficient, flexible and robust hybrid system is achieved. The study describes how the demonstrator is tested in real truck loading cycles. A detailed energy analysis is also presented to explain the energy flow inside the hybrid system.

ARTICLE HISTORY
Received 10 August 2017
Accepted 27 February 2018

KEYWORDS
Secondary control; digital hydraulics; multi-chamber cylinder

Introduction

Demands for increased fuel efficiency, reduced oil dependency and reduced exhaust gas emissions are important factors for both the on- and the off-highway automotive industry. For the off-highway industry, and not least for the construction equipment industry, the efficiency of hydraulic systems is of great importance in these matters. With a focus shifted towards energy efficiency, several new hydraulic components and techniques have been evaluated for use in different construction machines. In this paper, a new hydraulic series hybrid system based on hydraulic accumulators, secondary controlled motors and multi-chamber cylinders is proposed.

Secondary controlled hydraulics

Secondary-controlled systems are sometimes suggested as a basis for energy-efficient hydraulic system design, for instance by Palmgren and Palmberg (1988), Achten (2008), Pettersson and Tikkanen (2009), Busquets and Ivantysynova (2015). Secondary-control is ideally suited to rotary loads, using displacement control, where the relative displacement of a variable motor controls the relationship between a common pressure rail (CPR) pressure and torque. In applying this technology to construction machines however, there is clearly a need for solutions as to how the force of linear actuators should be controlled without introducing excessive throttling losses. One technique, described by for instance (Shih 1984, Achten and Palmberg 1999, Heybroek *et al.* 2012), is to use hydraulic transformers to 'transform' the CPR pressure to an arbitrary level in the hydraulic cylinder, without throttling. Bishop (2007, 2009) conceived a 'digital hydraulic' pressure transformer based on a double acting multi-chamber cylinder. An alternative, yet related approach is to skip the step of transforming pressure and instead utilise a multi-chamber cylinder to achieve a stepwise variable displacement linear actuator. Such a solution is studied in this paper.

The variable displacement linear actuator

The linear actuator investigated in this study is shown in Figure 1. It is designed and manufactured by the Finnish cylinder manufacturer Norrhydro OY. In this paper, we refer to this actuator as a 'Variable Displacement Linear Actuator', or VDLA. The naming is based on its capability to vary the displacement in a discrete manner by alternating the pressure connection of each chamber.

A simplified hydraulic schematic of the actuator is shown in Figure 2(a). Inside the four-chamber cylinder two positive forces are opposed by two negative forces. The sum of opposing forces depends on which pressure is applied to which cylinder area. The resulting hydraulic force, F_{hyd}, is given by

$$F_{\mathrm{hyd}} = p_{\mathrm{A}}A_{\mathrm{A}} - p_{\mathrm{B}}A_{\mathrm{B}} + p_{\mathrm{C}}A_{\mathrm{C}} - p_{\mathrm{D}}A_{\mathrm{D}}. \quad (1)$$

When all four cylinder areas differ in size and the CPR contains two pressure levels, the steady-state force combinations add up to $2^4 = 16$ steps. If a binary pattern is used when sizing cylinder areas

CONTACT Kim Heybroek kim.heybroek@volvo.com

Figure 1. VDLA from Norrhydro OY based on a four-chamber cylinder, valve manifold and an electric I/O control unit.

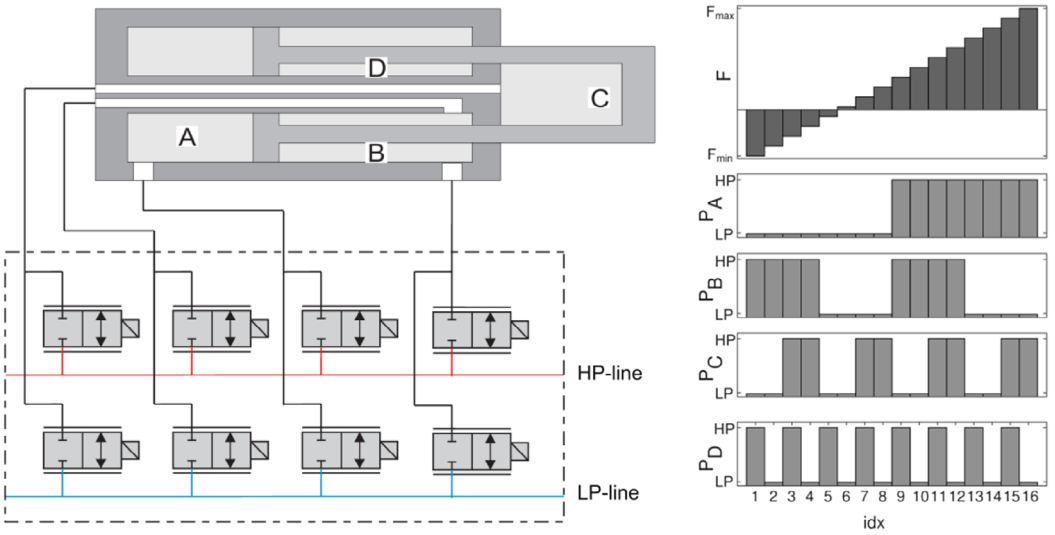

(a) Simplified schematic of the VDLA. (b) Static force spectrum

Figure 2. The VDLA schematic and its force spectrum.

A_A:A_B:A_C:A_D = $8A_D$:$4A_D$:$2A_D$:$1A_D$, all force steps in the spectrum become equal, as visualised in Figure 2(b).

Directly mounted onto the four-chamber cylinder is a valve manifold containing the necessary connections between its chambers and the CPR. On each connection, proportional valves are used for controlling the flow to and from each cylinder chamber. In principle the same concept, but instead based on on/off valves, was presented by Linjama *et al.* (2009), where the authors estimated a potential to reduce energy losses by 60% compared to a conventional load-sensing system. Since then, the technology has been investigated and further refined for several industrial applications, ranging from construction and material handling machines (Sahlman 2012, Dell' Amico *et al.* 2013, Heybroek and Norlin 2015) to aerospace applications (Belan *et al.* 2015) and large-scale wave-energy converters (Hansen *et al.* 2011, Hansen, 2014). The improvement in energy efficiency is from avoiding pressure compensation losses and enabling energy recuperation.

In a study by Huova *et al.* (2010) the idea of using different discrete force modes of a multi-chamber cylinder was combined with restriction control using several parallel-connected on/off valves. Hence, a higher force resolution was achieved in comparison to the pure force mode-based solution presented in Linjama *et al.* (2009), although at the cost of some extra losses. In the study by Sahlman (2012), a similar approach to restriction control was taken, but using conventional proportional valves instead of on/off valves. Wiktor and Heybroek (2014) and later so Heemskerk *et al.* (2015) suggested a control system based on a mix of proportional valves and on/off valves.

The baseline excavator

A typical crawler excavator motion system is illustrated in Figure 3.

In general, mass-produced hydraulic excavators are mature products that contain technical solutions iterated and refined over decades of development. Aspects weighed into its design are often a deliberate balance between several important factors such as safety, reliability, legislation, business models, fuel price and desired product features. However, as pointed out in several previous investigations (Pettersson and Tikkanen 2009, Inderelst *et al.* 2011), there is still plenty of room for improvement in terms of energy efficiency in the hydraulic systems. The single largest power loss normally comes from the inability to recover energy from overrunning loads, for instance during lowering of the boom or in deceleration of the swing motion. Another issue is the pressure compensation losses resulting from operating multiple functions with different pressure levels in parallel. In many excavator systems, this is addressed using two pumps working at isolated pressure levels whenever possible, and together only when needed

for faster operation of certain functions. Typically, the installed pump power capacity exceeds the combustion engine's power capacity. As the maximum torque of the combustion engine is then limiting the pump displacement, non-optimal efficiency of the pumps is frequent. Also, since high function velocities require high pump flows and small components are preferred over large components for cost reasons, the combustion engine is typically forced to operate at high angular speed where it has relatively poor efficiency and is noisier.

In many excavator duty cycles, the work power profile is transient and high power is seldom used over a long period of time (>5 s). All of the above-mentioned characteristics make the excavator an ideal application to 'hybridize' as proposed in the next section.

Proposed hybrid system

In Figure 4, a simplified schematic of the proposed system is shown. All linear drives are based on VDLAs and secondary-controlled hydraulic motors are applied to all rotary drives.

Using VDLAs for the work hydraulics eliminates the problem of losses in parallel operation since the effective cylinder area is adapted to the load condition of each function individually. Moreover, the VDLAs allow for energy recuperation from overrunning loads. Recovered energy may be used directly by the other functions, otherwise stored in the hydraulic accumulators connected to the CPR. The capacitance of the hydraulic accumulators 'decouples' the load side from the supply side as well as the individual loads from each other. This has the positive effect that the `supply system' (combustion engine and pumps) does not need to provide the peak power, which allows for downsizing. Considering these characteristics and how the hydraulic energy storage is placed in relation to the main energy flow, this system is commonly classified as a 'series hybrid'.

With a CPR as the backbone of the system, all rotary drives in the machine (the swing and the track drive) are based on secondary controlled motors. Using over-centre variable displacement hydraulic motors, four-quadrant operation is achieved. For a given CPR pressure the output torque is proportional to the motor displacement. Velocity is controlled by means of closed loop control based on feedback of measured angular velocity.

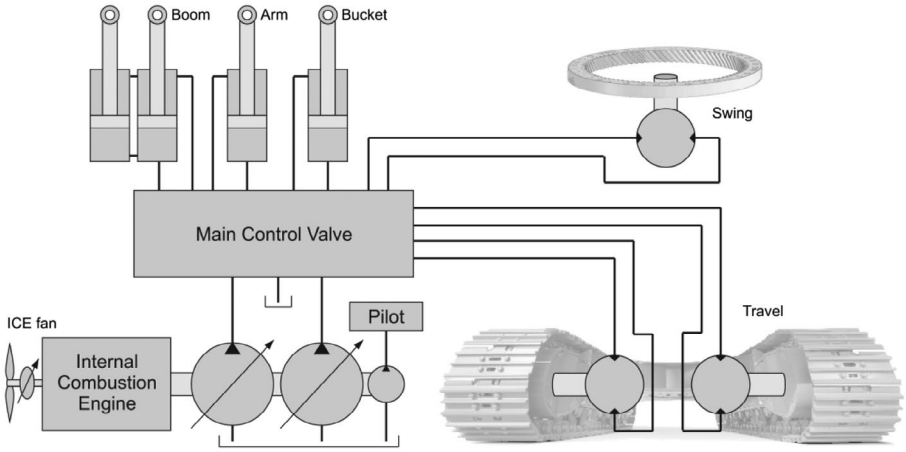

Figure 3. Simplified schematic of a crawler excavator hydraulic system, here considered 'baseline system'.

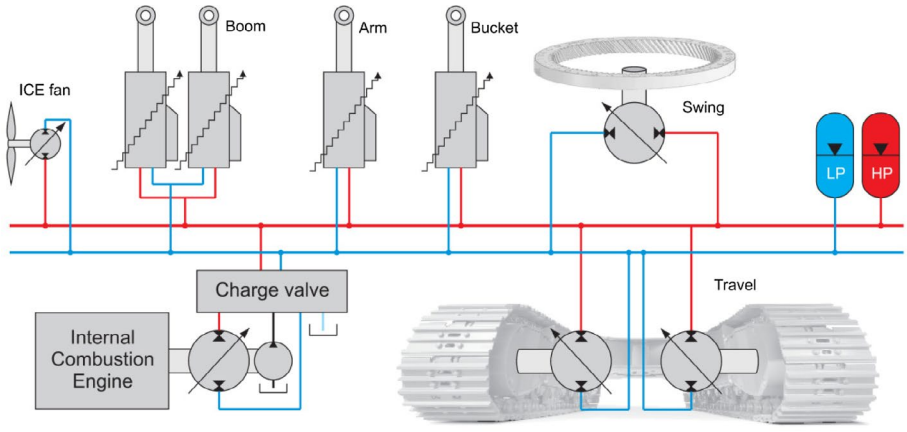

Figure 4. Simplified schematic of the proposed hydraulic hybrid system, in this study referred to as the 'hybrid system'.

Design process

The design process taken to develop the hydraulic hybrid described in this paper is illustrated in Figure 5, with the content of each phase described below.

I. Collect measurement data from a baseline machine operated in different working cycles. The actuator velocities and positions are acquired using position sensors. Actuator forces are estimated-based pressure sensor data. The engine RPM and torque load is acquired from the engine ECU.
II. Determine the power transfer of actuators, including their losses. The actuator dimensions are first determined based on recorded forces and designed pressure level. After this, the losses are estimated as a function of actuator dimensions and given velocities. Based on the calculated actuator powers, the CPR pressure variation is determined using an initial selection of supply side components (accumulator size and pump size). Energy is consumed from the accumulators when the total power requirement is higher than the supply side input power. The charge rate from the pump is set to zero when the maximum system pressure is reached. Actuator and supply side components sizing are iterated with the target to sustain the charge level of the accumulators that enables required output forces over a series of cycles. The minimum pump size is often determined by the travel function, discussed later. When a preliminary selection of components is made, a first evaluation of energy efficiency is possible.
III. Dynamic simulation is used to get a better understanding of the system behaviour and a main target is to capture energy losses not accounted for in the static analysis. This phase includes building up a model of the machine structure and models of all the main hydraulic components (pumps/motors, accumulators, valves and cylinders). Measurement data from the baseline machine are used for generating reference signals to the dynamic simulation where the objective is to achieve as similar mechanical work as possible.
IV. In this final phase, the resulting design is evaluated in the physical machine which is tested in relevant duty cycles. Here, tuning for operability is an essential constituent where testing is carried out by several operators to consider the variation in operator behaviour.

In this paper, the main focus is on phase IV and also parts of phase III are covered to describe the basic working principles of the VDLA and supply system control. Phase III is included to demonstrate the most essential part of the design process and to highlight that fairly simple models can be used in the dimensioning of a VDLA-based hybrid system. Since the design process focuses on achieving the same work output as that of a conventional machine it does not account for the new possibilities of a hybrid system, such as improved productivity. The simulation results from Phase III are therefore not compared to the measured results in Phase IV. Instead, the more relevant comparison is made between a reference machine and the proposed hybrid machine.

Simulation

The main purpose of the simulations carried out in this study is to get a first estimate of energy saving potential and a basis for component dimensioning for the design of a full-scale demonstrator. The system model is developed for 'backward-facing simulation', where cycle data from an EC300E Volvo CE excavator are used. The cycle data is measured in South Korea based on machine operation using professional operators. The studied duty cycle is the so called 'digging-and-dumping cycle' where the excavator is used for loading gravel onto a load receiver which is standing on the same level as the excavator. To dump material into the load receiver the excavator slews 90 degrees from where it is digging. The material used in the test is gravel with a standard fraction 30–50 mm. This section describes the main sub-system models used in simulation. All models are developed in Matlab Simulink.

Machine structure model

The excavator mechanism is modelled in three dimensions where the main input parameters such as joint locations, link masses and centres of gravity are taken from manufacturing drawings. An illustration of the machine and its representation in Matlab's SimMechanics is shown in Figure 6.

The cylinders are modelled as two separate bodies connected with a prismatic joint. The couplings between the hydraulic cylinder models and the structure model are handled with prismatic joints. Each prismatic joint

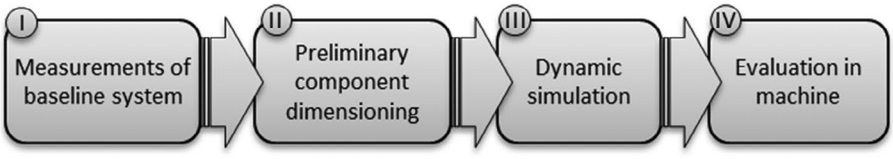

Figure 5. Overview of the design process used in the design of the hydraulic hybrid.

takes the force, generated by the hydraulic cylinder model, less friction, as input and provides cylinder stroke and velocity as output. These outputs are inputs to the hydraulic cylinder model. To describe the cylinder friction, a modified Stribeck friction model, proposed in Andersson *et al.* (2007), is applied as

$$F_\mu = \tanh\left(K_f v_p\right)\left[F_C + \left(F_S - F_C\right)e^{-\left(\frac{v_p}{v_s}\right)^2}\right] + bv_p, \quad (2)$$

where F_μ is friction force, v_p which is the piston velocity, F_c the Coulomb friction force, F_s is the maximum static friction force, v_s is the sliding velocity coefficient, b is the viscous friction coefficient and K_f is a coefficient that determines the transition rate of the tanh-function from near −1 to near 1.

The parameters used in the friction model are set so that similar actuator power behaviour is observed from the simulation model as seen in the *return-to-dig* portion of the working cycle in the measurement. The return-to-dig here refers to machine operation where boom is operated back to the position where digging motion can start after emptying the bucket.

The coupling between the hydraulic model of the swing unit and the structure model is handled with a revolute joint which gets torque from the hydraulic model, less the swing friction, as input and provides swing unit angular velocity as output. The friction model used for swing is the same as for cylinders but using torques and angular velocities, and a different set of coefficients. As all mechanical work performed by swing is friction work in the observed working cycle the swing friction model parameters are set so that mechanical output from the simulation model is matched with the measurement data.

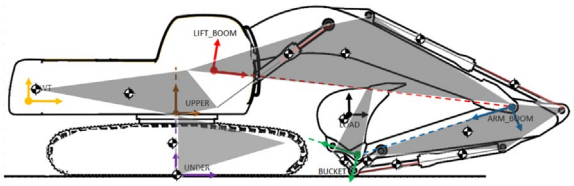

Figure 6. Coordinate systems defined in the model. The grey blocks show the system representation in SimMechanics.

Ground model

The reaction force in ground interaction is modelled as a disturbance force, F_{dist}, per actuator, as a function of bucket angle. The link between disturbance force and bucket angle is estimated separately for each function by fitting an average curve to the measured values. Figure 7 shows the fitted functions for each actuator.

When the ground contact ends, external forces are set to zero and an inertia load is applied to the bucket. The transition points and load masses are analysed and set separately for each working cycle. The measured motions are simulated without a ground model and the measured forces are compared to the simulated forces to identify the ground contact activation points. The ground contact deactivation points are determined from bucket and arm forces as those rapidly decrease as digging ends and bucket is lifted from the ground. The load mass for each working cycle is estimated from the measured lifting force. The ground model and estimated loads are fine-tuned for each working cycle by multiplying the reaction forces and load estimates with near 1 coefficient so that simulated and measured mechanical forces and velocities correlate well, leading to a good match in mechanical energy at the end of an observation interval. The resulting forces and masses used in the simulation are shown in Figure 8. The drawback of this approach is that the ground model is too simplistic for any kind of variation in the digging behaviour. This means for instance that the cycle time is locked and different levels of productivity cannot be evaluated. Naturally, there are more sophisticated approaches to ground modelling if such analysis is desired, e.g. see Filla (2015).

VDLA model

The multi-chamber actuator comprises a set of individual single-chamber systems, mechanically linked together through a movable piston. The physical properties for one of these chambers are shown in Figure 9.

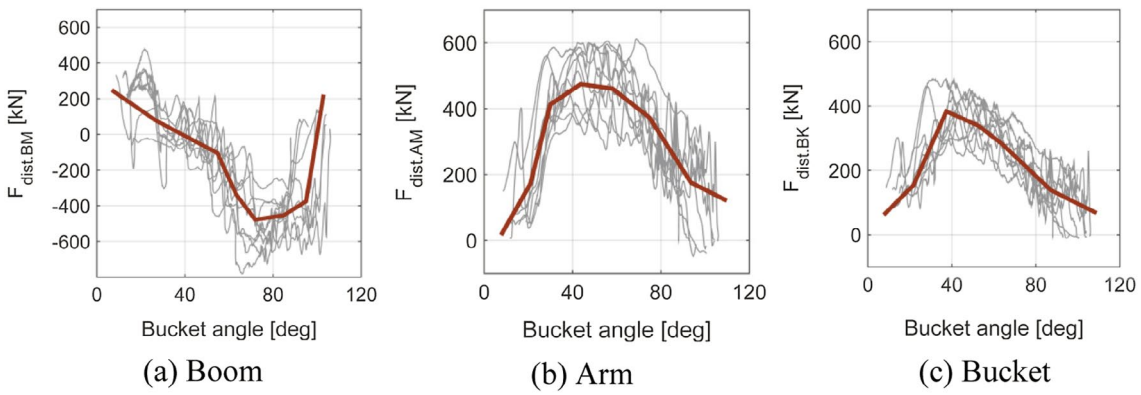

Figure 7. Estimated ground contact forces as a function of bucket angle used in the simulation model.

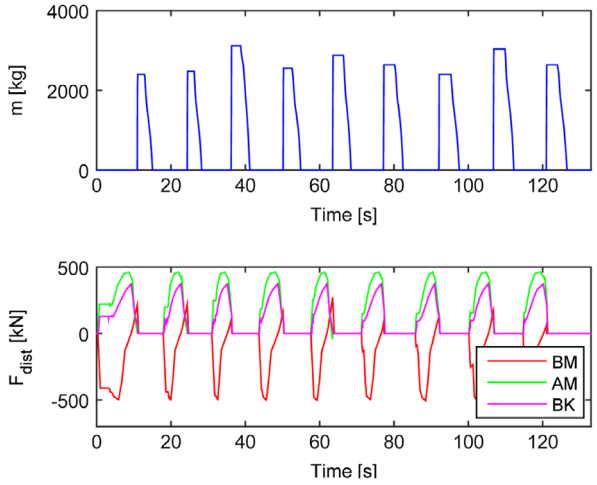

Figure 8. Simulated load mass and external force disturbance per function due to ground interaction.

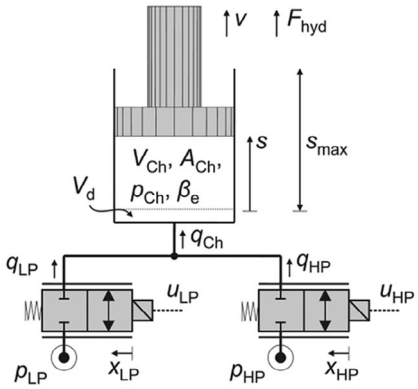

Figure 9. Model properties for a single-chamber actuator.

Of notational convenience the actuator force in (1) is expressed in vector form as

$$F_{\text{hyd}} = A_{\text{Ch}}^{T}\varphi_{\text{dir}}p_{\text{Ch}}, \tag{3}$$

where A_{Ch} and p_{Ch} are column vectors containing the cylinder chamber areas and pressures, respectively. φ_{dir} is a diagonal matrix that defines the direction for each force component based on the cylinder geometry. The pressure dynamics in the cylinder chambers are described by

$$\dot{p}_{\text{Ch}} = \beta_e V_{\text{Ch}}^{-1}\left(q_{\text{Ch}} - \varphi_{\text{dir}}A_{\text{Ch}}v_p\right), \tag{4}$$

where β_e is the hydraulic bulk modulus, v_p is the piston velocity. The chamber volume, V_{Ch}, is a function of the piston stroke, s and the maximum piston stroke, s_{max} as

$$V_{\text{Ch}} = \left(\frac{s_{\text{max}}}{2}\left(I_4 - \varphi_{\text{dir}}\right) + s\varphi_{\text{dir}}\right)\text{diag}\left(A_{\text{Ch}}\right) + V_{\text{d}}, \tag{5}$$

where V_d is the dead volume. V_{Ch} and V_d are diagonal matrices and I_4 is the 4×4 identity matrix. The chamber flows, q_{Ch}, are given by

$$q_{\text{Ch}} = q_{\text{s,LP}} + q_{\text{s,HP}}, \tag{6}$$

where $q_{\text{s,LP}}$ and $q_{\text{s,HP}}$ are the flows from the low- and high pressure supply lines, respectively, calculated as

$$q_{s,j} = \text{sgn}\left(p_{s,j} - p_{\text{Ch}}\right)K_{v,j}x_{v,j}\sqrt{\left|p_{s,j} - p_{\text{Ch}}\right|}, \quad j \in \{\text{LP,HP}\}, \tag{7}$$

where all mathematical operators work element-wise. K_v is a lumped parameter that describes the flow resistance for a hydraulic valve. The supply pressure $p_{s,j}$ varies with accumulator charge, described later. The valve opening is described by a normalised quantity, x_v with dynamics relative to an electric control signal u as

$$\dot{x}_{v,j} = \frac{1}{\tau_v}x_{v,j} + \frac{1}{\tau_v}u_j, \quad j \in \{\text{LP,HP}\}. \tag{8}$$

Disregarded characteristics in this model are the effects of time delays in the electric control as well as the hydrodynamic flow forces that typically result in a power limitation of hydraulic valves. Moreover, `dead zones' in the valves are disregarded.

Accumulator model

Both accumulators are modelled separately assuming an adiabatic process for charging and discharging. The accumulator capacitance is assumed to represent the complete compressibility of the CPR and by neglecting the flow losses in hydraulic lines and mechanical friction in the accumulator, the supply line pressure is assumed equal to the gas pressure of the accumulator. Thus,

$$p_{s,j} = \frac{p_{0,j}V_{0,j}^{\gamma}}{V_{g,j}^{\gamma}}, \quad j \in \{\text{LP,HP}\}, \tag{9}$$

where p_0 is the accumulator pre-charge pressure, V_0 is the total accumulator volume. The polytropic index γ is assumed constant at a value of 2.3. The gas volume, V_g is given by

$$V_{g,j} = V_{0,j} - \int q_{\text{acc},j}dt, \quad j \in \{\text{LP,HP}\}, \tag{10}$$

where $q_{\text{acc},j}$ is the flow to the accumulator on pressure line $j \in \{\text{LP, HP}\}$, described as

$$q_{\text{acc},j} = q_p - \sum \text{Q}_j - q_{\text{sw}}, \tag{11}$$

where q_p is the flow produced by the supply pump, $Q_j = \left\{q_{s,j}^{\text{BM}}, q_{s,j}^{\text{AM}}, q_{s,j}^{BK}\right\}$ is the flow to the respective VDLAs and q_{sw} is the flow to the swing motor.

Pump/motor model

The main pump and the swing motor are modelled with the standard torque, $T_{p/m}$, and flow, $q_{p/m}$, relations assuming a constant cycle efficiency factor as

$$T_{p/m} = \frac{\in D\left(p_{s,\text{HP}} - p_{s,\text{LP}}\right)}{2\pi\eta_{\text{hm}}^{k}}, \tag{12}$$

$$q_{p/m} = \in D\omega\eta_{\text{vol}}^{k}, \tag{13}$$

where $\in$ is the relative displacement, D is maximum displacement and $k = \pm 1$ depending on if the unit is operated as pump or motor. The volumetric efficiency η_{vol} and the hydromechanical efficiency η_{hm} are both assigned a constant value of 0.9. The displacement dynamics are modelled with a first order transfer function as

$$\dot{\in} = \frac{1}{\tau_\varepsilon} \in + \frac{1}{\tau_\varepsilon} u_{p/m}, \tag{14}$$

with a time constant $\tau_\varepsilon = 100$ ms.

Control aspects

The challenges in control for this hybrid system range from the lowest level in how individual valves are controlled to the highest machine level. Since the focus of this paper is to evaluate the concept on machine level, the in-depth description of component controls is deliberately left out, including the force control principles of VDLA's as well as the details of secondary control. For more information, see referenced literature in the introduction.

VDLA controls

The control approach taken for the VDLAs is based on closed-loop velocity control coupled with machine model and pressure transducer data to generate a force reference for each actuator. The actuator thus includes pressure sensor for all chambers and a piston stroke sensor. The force references are further split into individual chamber pressure references. The supply line pressures are measured and individual valve openings are calculated with a model-based approach using pressure and flow references.

The main goal in the force control is to minimise the resistive losses in valves. The resistive losses can be split into two separate categories:

(1) Throttle losses – occur from the pressure drop caused by hydraulic flow resistance at a stationary pressure ($\dot{p}_{\text{Ch}} = 0$) during piston motion ($v \neq 0$).
(2) Switching losses – occur when transitioning from one force mode to another due to fluid compressibility.

The throttle losses are minimised by controlling the cylinder with valves fully open or closed, i.e. on/off control. A simple approach to this is to choose the force index that yields the steady-state force closest to the reference, F_{ref}, i.e. the force $\mathrm{F}[\mathrm{idx}]$ that minimise the tracking error. To avoid jittering when F_{ref} is equally close to two consecutive force steps, a hysteresis is added.

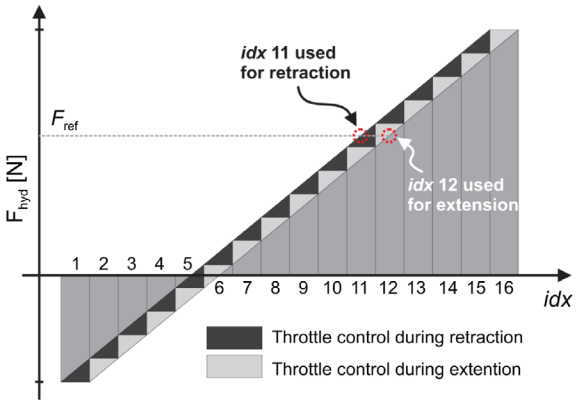

Figure 10. Illustration of the VDLA force spectrum and how throttle control is used within force states, denoted idx in the diagram.

Since proportional valves are used, it is possible to apply throttle control within each force mode, as illustrated in Figure 10. This is useful when accurate speed control is required and also in transitions between the 16 force steps. Since accurate speed control is normally needed only at low velocities, the pressure drop has relatively low impact on energy consumption since the flows are low. If the closest force mode is consistently selected, the throttle losses will be limited to one step size and are half a step size on average.

The controller selects between secondary control and actively balanced throttle control based on logic that considers joint inertia, cylinder force and velocity. Figure 11 illustrates VDLA control behaviour in simulations. To generate velocity references for the closed loop velocity controls of actuators, an outer position control loop is used which is based on position P-controller and a feedforward term from measured velocity. The simple position control approach is selected since the simulation focuses on matching the total mechanical output energy with the measurement at the end of the observation interval. The mechanical output energy is calculated by taking a sum from the integrated actuator output powers. The actuator output power calculation is based on actuation velocity and pressure difference over the actuator.

The poorly dampened ground model causes slight ripple to the actuator velocities when the ground contact model is active, as shown in Figure 12 at simulation time 5–10 s. At simulation time 18s, the discrete activation of ground contact causes velocity tracking error. The velocity tracking error comes from the rapid increase in the required actuation force as the ground model activates. This behaviour is not seen as an issue as very simplified ground model is used and good enough correlation between measured and simulated actuator output power behaviour is reached for component sizing. The slight ripple and tracking error have minor effect to the overall losses.

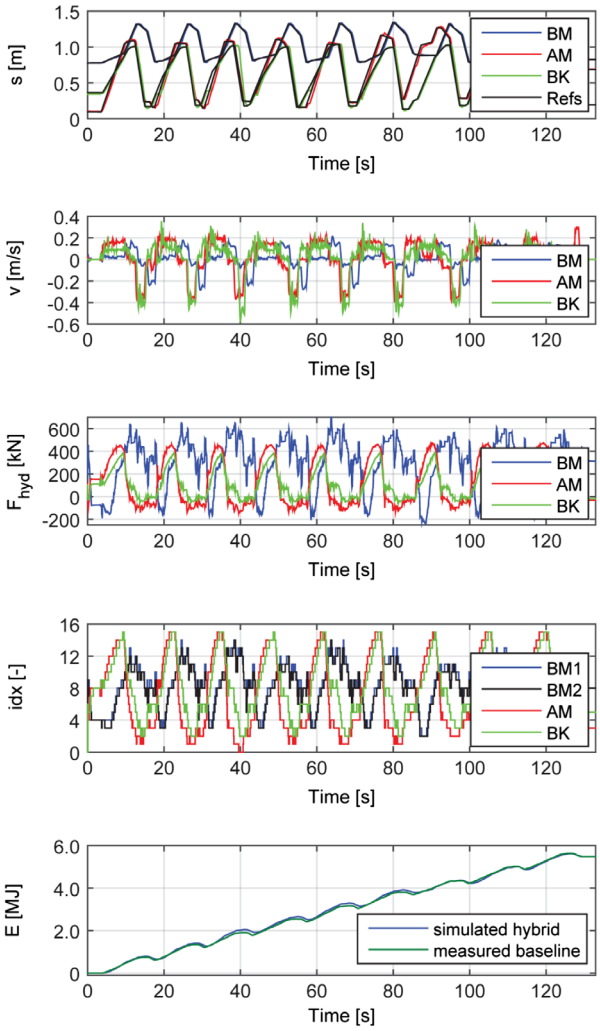

Figure 11. Output energy, $E_{hyd} = \int v_p F_{hyd}$, tracking performance in simulations and other related quantities such as the selected force index, idx.

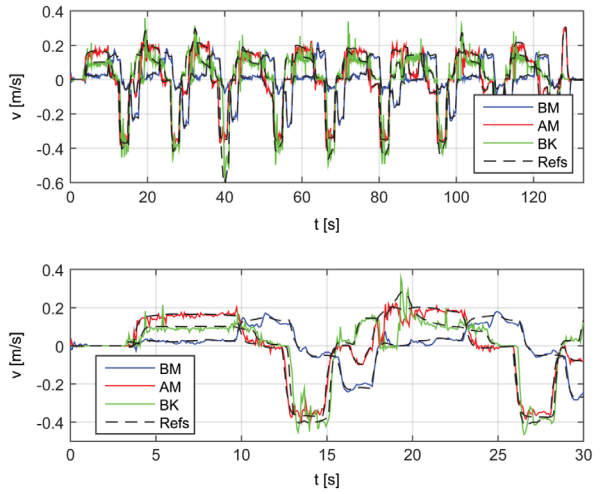

Figure 12. Velocity tracking. The disturbance in velocity tracking is caused by the discrete activation of ground contact at $t = 18$ s.

Supply system controls

The basic idea is to determine the supply line pressure level reference based on the potential energy of the boom system and use hysteresis control to command flow from the fixed displacement charging pump. Flow is taken from the LP-line and supplied to the HP-line. When charging is requested, logic valves connect the pump discharge port to the HP-line otherwise oil is circulated back to its suction port. Figure 13 illustrates the basic function of the supply system in the simulation. The result shows that the pump is frequently charging the HP-line which reflects that the system is near its capacity limit. Furthermore, it highlights the CPR pressure variation as a consequence of the accumulator charge.

VDLA:s and motors attached to the CPR can directly draw energy from the accumulators, allowing for a higher output power compared to the baseline machine where the power is limited by the pumps. To avoid draining the accumulators, a software-based power management strategy is introduced. The strategy targets high and steady power availability, where the power distribution between functions is easily configurable from a graphical user interface.

Hybrid system integration

Based on results from the simulations all necessary system components are dimensioned and a full-scale proof-of-concept demonstrator is built up based on a 30-ton class crawler excavator from Volvo CE (model EC300E). Due to the estimated peak power reduction, a diesel engine with 25% lower gross power rating is installed. The limitation for engine downsizing is mainly the need for high continuous power for the track drive. However, with the proposed system solution, high travel speeds are still possible when travelling on flat ground, but maximum operating power is naturally limited by the smaller engine. Since focus of this paper is on a cycle where travel function is not used, the detailed description of this drive is excluded from the scope of this paper.

The installed pump capacity is reduced by approximately 40% compared to the base machine. The linear actuators are sized for an equivalent performance at the nominal CPR pressure level.

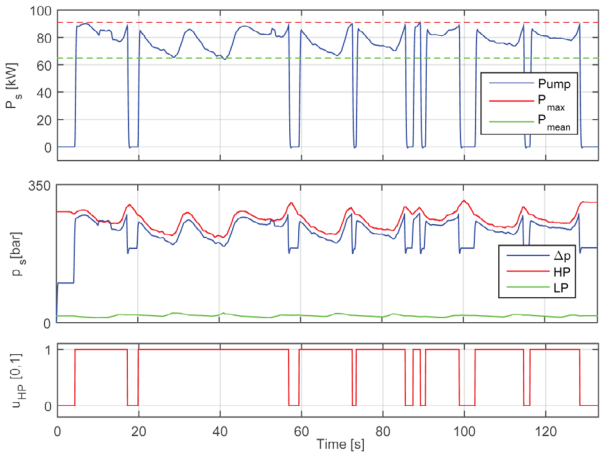

Figure 13. Hydraulic charging behaviour and accumulator characteristics in simulation.

The CPR system greatly simplifies installation in the machine as each function simply connects to the two pressure lines of the CPR, resulting in fewer pipes and hoses on the work implement. The hoses from the main pump are also smaller since the pump is operated in a closed loop and is no longer required to provide peak power. Moreover, since the new system is designed for electronic control, the current rather complex hydraulic pilot circuitry may be simplified by electric joystick control.

The accumulator size depends heavily on which supply system is used and how it is controlled. In the demonstrator $V_{0,j}$ = 100 L is used. In the excavator, there are several locations where hydraulic accumulators can be placed, especially when a downsized diesel engine is used. In the hybrid demonstrator, the accumulators are temporarily placed on the outside of the counter-weight.

The secondary controlled swing drive is based on an over-centre closed circuit axial inline piston pump/motor. The time constant of the unit is about 100 ms similar to what was used in simulation. The approach has high operating efficiency and good control behaviour in general motions. The main control challenges relate to gear system play, low velocity operation and consistent braking performance. To ensure consistent braking performance with varying CPR pressure, a valve was installed to the swing unit HP inlet. The gear system play reduces the maximum allowable control gains of the closed-loop PID controller due to low inertia while operating inside the play.

Practical tests

The hydraulic hybrid demonstrator is extensively tested by four professional operators in tests side-by-side a standard excavator of the same make and weight class (Figure 14).

Test method

As described by Frank *et al.* (2012), the fuel consumption of a working machine is strongly influenced by three factors:

(1) Machine specification.
(2) Working environment.
(3) Operator behaviour.

In this study, the influence of an updated machine specification is of main interest. To minimise variation in working environment, parameters such as machine positioning, digging material, shape of the gravel pile, etc., are closely monitored by experienced test personnel at Volvo CE. To understand the effects of operator behaviour, several operators are used.

In this paper, the focus is on a digging and dumping cycle, described earlier. The test is carried out as follows:

Each test consists of 5 runs, where each run means dumping 5 buckets of gravel into the load receiver. After each run, the load receiver is weighed and the average bucket load is calculated. Fuel consumption is measured both by the engine management system (based on injection times) and by a separate fuel measurement device, and the average cycle time is calculated based on the total time for each run. Based on this, the fuel rate in litre/s, the productivity in ton/s and the fuel efficiency in ton/litre are calculated.

Test results

The baseline machine was operated in 'H-ECO' mode, which is considered the most fuel-efficient setting, given the work at hand. One operator also tested the machine in the so called 'P-MAX' mode, providing the highest possible productivity.

In Figure 15, the results are compared on an individual level, where every run from the hybrid machine is compared to every run of the baseline machine, using

Figure 14. The hydraulic hybrid demonstrator in action.

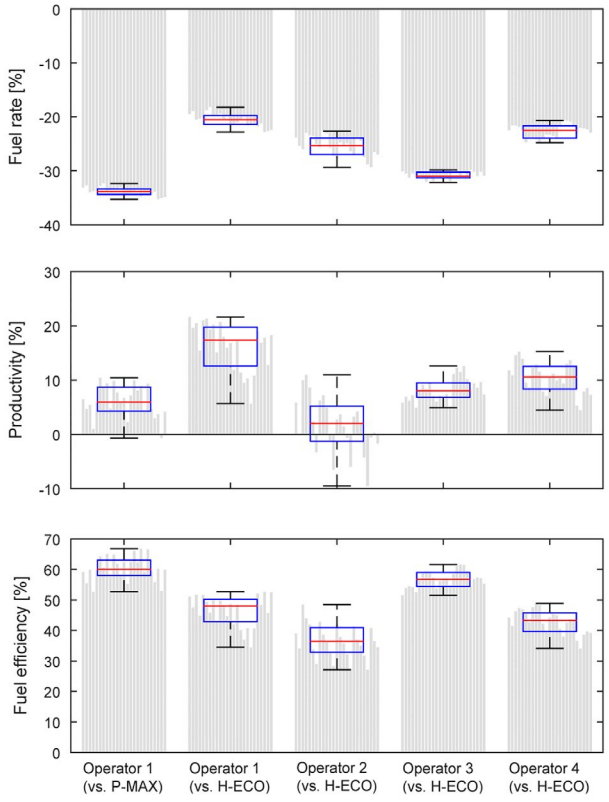

Figure 15. Performance improvements in terms of increased productivity, reduced fuel rate and increased fuel efficiency.

the same operator on both machines. This gives 25 comparisons per operator test. The boxes shown in the figure have a red mark to show the median value, while the edges of the box are the 25th and 75th percentiles and whiskers that extend to the extreme data points. As seen from the result, the fuel efficiency improvement is at its greatest when comparing to P-MAX mode, with a mean value of 60%. In H-ECO mode, operator 3 demonstrates the greatest improvement with a mean value of 56%. Operator 3 also shows the smallest dispersion in results. Noteworthy is that the dispersion in improvement is considerable between the different operators, due to the difference in operator behaviour, which is also a conclusion by Frank *et al.* (2012).

Another view of the results is found by comparing all tests to each other, irrespective of who operated the machine. During the testing and tuning period, the baseline machine is tested in 41 runs in total, while the hybrid is tested in 110 runs in total. Comparing all samples of the baseline machine to all the samples of the hybrid machine gives 4510 comparisons. Based on this, the results are plotted as histograms and cumulative distribution functions in Figure 16. In this data-set, several different tuning parameters were used on the machine, in some cases in favour of improved productivity and sometimes in favour of reduced fuel consumption. It is important to note that this distribution includes the full range of comparisons (e.g. best hybrid to worst baseline, best baseline to worst hybrid).

Energy analysis

Two test runs from Operator 1 is selected for deeper analysis. For the base machine, a run in P-MAX mode is selected for easier comparison since cycle times are similar to those of the hybrid. As shown in Figure 17, the hydraulic output power and mechanical work of the two machines is similar which supports the claim that the comparison between the two machines is relevant. The mechanical work of the hybrid machine is slightly higher, which is reflected by an increase in productivity, discussed later.

In Figures 18 and 19, some relevant system properties are compared between the hybrid machine and the baseline machine. In Figure 18, the difference in supply system function is visualised. In the baseline machine two electronically controlled pumps are used together with an open-centre main control valve. The pressures of the baseline system have a transient behaviour depending on the actuator load, while in the hybrid system the pressures are changing with the accumulator charge. In the cycle, the maximum pump flow is occasionally utilised but more frequently they are operated with a partial displacement setting. For the hybrid system, the maximum flow capacity is

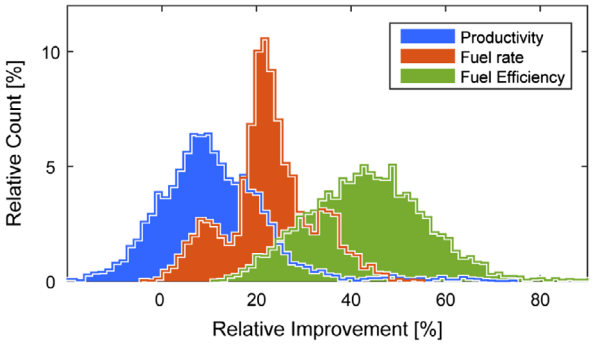

Figure 16. Histograms showing the test result distribution.

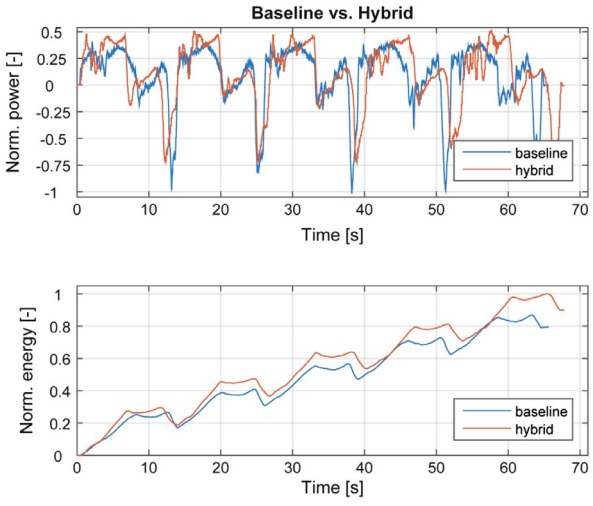

Figure 17. Load-side hydraulic power (top) and the cumulative load-side energy (bottom). All quantities are normalised.

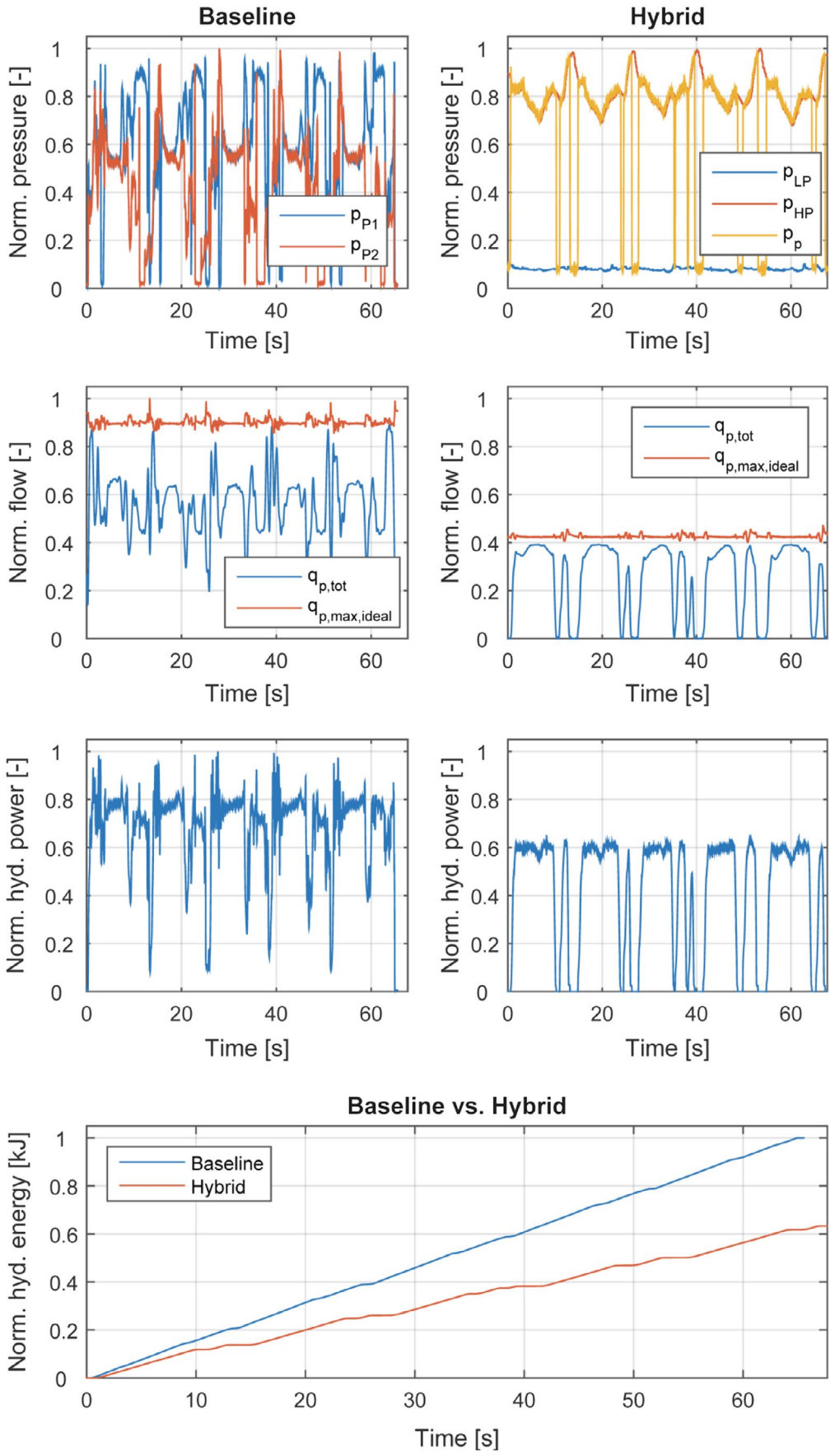

Figure 18. Hydraulic supply system operation. The graphs to the left show the baseline machine while graphs to the right show the hybrid machine. All quantities are normalised.

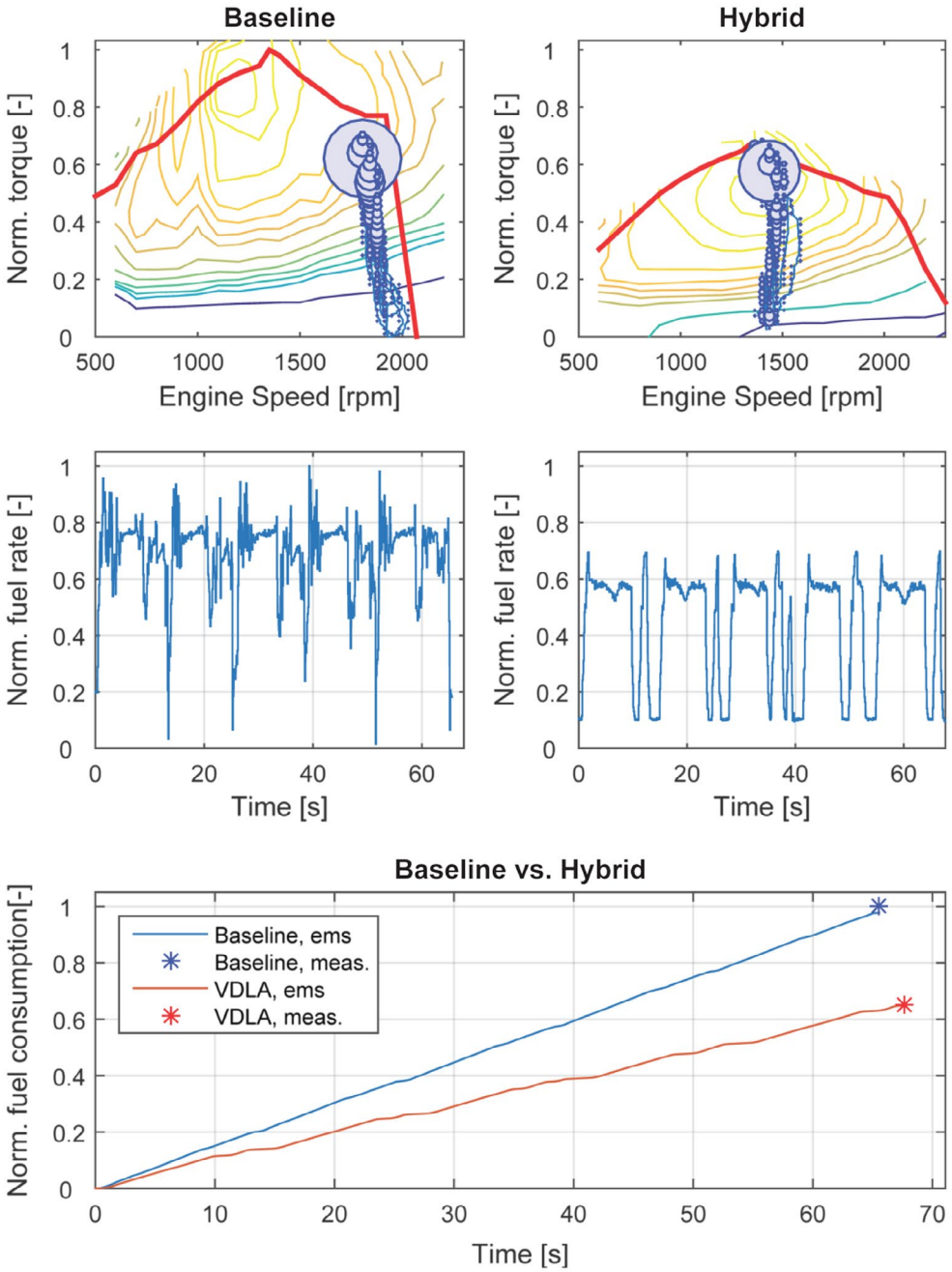

Figure 19. Combustion engine operation. The graphs to the left show the baseline machine while graphs to the right show the hybrid machine. All quantities are normalised.

~55% lower than of the baseline system which is fully utilised when flow is commanded. In the baseline machine, there is a strong coupling between hydraulic supply power and load power, while in the hybrid system accumulators decouple the supply side from the load side. Furthermore, in the hybrid system, all functions support energy recuperation, which in combination with the hydraulic accumulator permits the use of a smaller and less dynamic supply system. As shown in the bottom graph, the hydraulic pump's output energy is reduced by approximately 35% compared to the baseline machine.

The resulting operation of the combustion engine is shown in Figure 19, where the driveshaft output torque is denoted T_{ICE} and the angular speed is denoted n_{ICE}. The contours in the top graphs represent the efficiency levels of the combustion engines. The thick red line is the engine's maximum torque curve and the bubbles' size indicates how much time is spent at different operating points. In the hybrid machine, the smaller engine runs at a lower angular speed, bringing it closer to its 'sweet-spot' in efficiency. The graph below shows the resulting fuel rate, as calculated by the engine management system (ems). The bottom graph shows the cumulative fuel consumption integrated from the ems' fuel rate signal. As an extra verification of this result, the graph also shows the value, marked by an asterisk, taken from the separate fuel measurement system in the end of the cycle.

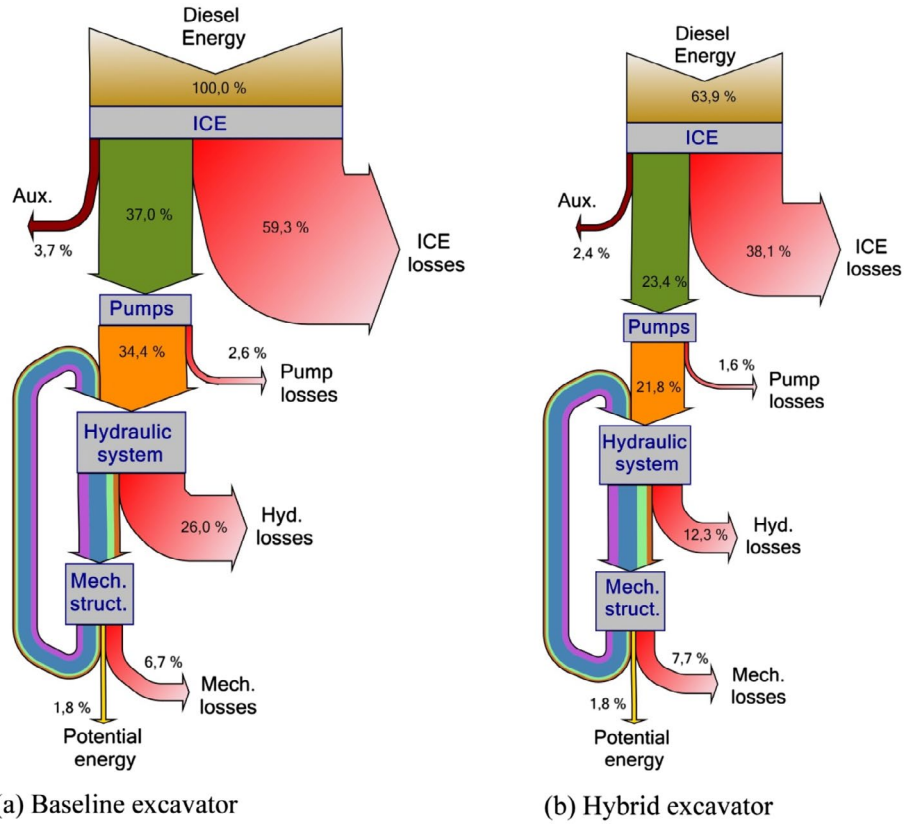

Figure 20. Energy flow of the two machines in the truck loading cycle. For easier comparison between the two, all percentage figures are given in relation to the input energy in (a).

Figure 20 provides a high level comparison of the energy flows within the two machines for the same test cycle. In the figure, the mechanical losses are defined as mechanical output energy less the potential energy. The potential energy is calculated by multiplying the measured weight with an estimated lifting height. The start height for lifting was set as midway in the ground motion and the end height was set as the bucket reaches half stroke during dumping. The pump losses are estimated based on a fixed efficiency of 93%. The energy that is circulated from the mechanical structure back to the hydraulic system represents the negative work. In the baseline system this energy is turned to hydraulic losses, while in the hybrid system part of the energy is recuperated. An interesting note is that the combustion engine of the hybrid system has a worse efficiency even though it is operated in its efficiency sweet spot. This is due to the use of a different engine which has a lower maximum efficiency.

Figure 21 dives deeper into the energy flows of the hydraulic hybrid system, where the input and output energies in this graph correspond to those in Figure 20(b).

The pump input energy, denoted A in the figure, is calculated from the measured pump pressures and flow rates. The resistive work (B) and regen. work (C) are calculated from the measured velocities and port pressures. First-order dynamics is assumed for the swing motor when calculating its relative displacement based on its reference signal. The energy consumed (D) from and returned to the CPR (E) is calculated from the estimated flow rates and the measured line pressures. An actuator chamber flow rate is estimated from a measured velocity, chamber pressure and valve command. The chamber pressure is used for identifying flows due to fluid compression and valve command for identifying the CPR line connection. The accumulator output flow is estimated by subtracting the sum of actuator flow rates from the pump input flow. Flow is required from the accumulators when the difference is negative. The accumulator energy losses and input energies (F) are calculated from the estimated accumulator output energies (G) using a fixed efficiency of 90%. The accumulator state of charge difference (SOC diff.) is calculated from the measured line pressure levels at the beginning and end of the measurement. The CPR losses contain supply line flow losses, pressure relief losses and leaks from the CPR. Also, the unidentified part of losses, i.e. the difference between pump input energy less the mechanical work and estimated losses, is here counted as CPR losses.

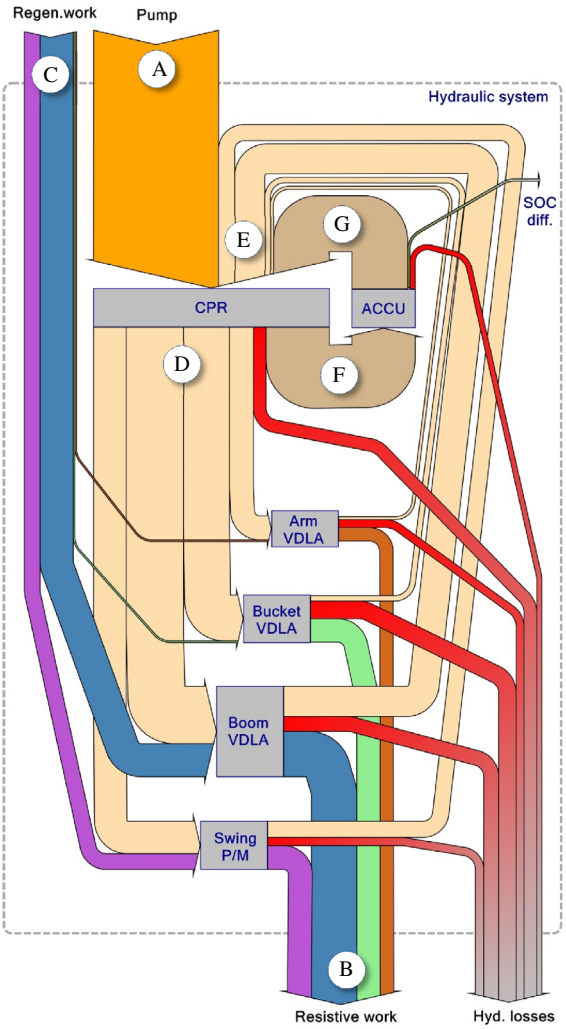

Figure 21. Detailed energy flow inside the hybrid hydraulic system.

Conclusions

A new type of hydraulic hybrid system was designed, simulated, implemented and tested in a 30-ton class crawler excavator. The hybrid system uses variable displacement linear actuators, secondary controlled pumps/motors and hydraulic accumulators all connected to a hydraulic CPR system powered by a downsized combustion engine.

The system was tested in a typical truck loading cycle, side-by-side against a standard production machine of the same brand and weight class. Overall the simulation showed good correlation with measurements. The largest deviation was in the swing where additional valve had to be installed to reach the required performance level. Measurement results show an improvement in fuel efficiency (ton/litre) in the range 34–50% for all comparisons made in the interquartile range. In the 10th percentile of comparisons, the improvement is greater than 58%. The dispersion in results depends on the difference in operator behaviour and in which working mode of the baseline machine comparisons are made. The improvement derives from a combination of reduced fuel consumption and augmented productivity. The reduced fuel consumption is mainly due to reduced losses in the hydraulic system, where the main contribution comes from energy recovery in boom down motions and swing deceleration. The productivity increase is a result of greater power availability, which enables faster multi-function operation. All drives in the hybrid system are based on electronic sensor feedback control, leading to highly configurable machine behaviour. Even though the important aspect of system cost was not included in this study, it is noted that the suggested approach leads to simplified and modular system structure.

List of notations

Quantity	*Description*	*Unity*
β_e	Effective fluid bulk modulus	Pa
η_{vol}	Volumetric efficiency	–
η_{hm}	Hydro-mechanical efficiency	–
ε	Relative displacement of pump/motor unit	–
γ	Polytropic exponent	–
τ	Time constant for valve	s
φ_{dir}	Force direction matrix	–
A_{Ch}	Cylinder chamber area vector	m^2
A_j	Hydraulic area, $i \in \{A, B, C, D\}$	m^2
b	Viscous friction coefficient	Ns/m
D	Maximum displacement of pump/motor	m^3
F_c	Columb friction force	N
F_s	Maximum static friction force	N
F_{hyd}	Hydraulic force	N
F_μ	Friction force	N
E_{hyd}	Hydraulic energy provided to actuators and swing	J
K_v	Lumped flow coefficient	$m^3/(s\sqrt{Pa})$
K_f	Coefficient that concerns the friction force	Ns/m
P_s	Supply power	W
p_{Ch}	Chamber pressure	Pa
$p_{s,j}$	Supply pressure, $j \in \{$ LP, HP $\}$	Pa
Q_j	A set containing the flows to the accumulators	m^3/s
$q_{acc,j}$	Flow to accumulator connected to $j \in \{$ LP, HP $\}$	m^3/s
q_{sw}	Flow to the swing drive	m^3/s
$q_{p/m}$	Flow from/to pump/motor	m^3/s
$q_{s,j}$	Flow to chamber from supply line $j \in \{$ LP, HP $\}$	m^3/s
q_{Ch}	Chamber flow	m^3/s
s/s_{max}	Piston stroke / max stroke	m
$T_{p/m}$	Torque of pump/motor	Nm
$T_{ICE\|ICE}$	Torque load on the combustion engine	Nm
u	Normalised control signal to valve	–
V_{Ch}/V_d	Chamber volume / Dead volume	m^3
$V_{0,j}$	Total accumulator volume connected to $j \in \{$ LP, HP $\}$	m^3
$V_{g,j}$	Accumulator gas volume connected to $j \in \{$ LP, HP $\}$	m^3
v_s	Sliding velocity coefficient	m/s
v_p	Piston velocity	m/s
n_{ICE}	Rotational speed of the combustion engine	rev/min
$x_{v,j}$	Normalised valve opening to $j \in \{$ LP, HP $\}$	–

Acronyms/subindex

Acronym	*Description*
CPR	Common Pressure Rail
VDLA	Variable Displacement Linear Actuator
HP	High pressure
LP	Low pressure
SOC	State of Charge
idx	Force index
BM	Boom function
AM	Arm function
BK	Bucket function
SW	Swing function
acc	Accumulator
ICE	Internal Combustion Engine

Disclosure statement

No potential conflict of interest was reported by the authors.

Funding

This work was supported by the Vehicular Research Program (FFI) in the Swedish Energy Agency under Grant [39367-1].

Notes on contributors

Kim Heybroek was born in Västervik, Sweden, in 1981. He received his MSc degree in Mechanical Engineering from Linköping University (LiU), Sweden in 2006. In 2008, he joined Volvo Construction Equipment in Eskilstuna where he is currently working. In 2017, he received his PhD degree at the Department of Fluid Power and Mechatronic Systems at LiU.

Mika Sahlman was born in Pyhäselkä, Finland, in 1987. He received his MSc Degree in Mechanical Engineering from Tampere University of Technology (TUT), Finland in 2012. Later that year, he joined Norrhydro's R&D team in Tampere where he is currently working as a Systems Engineer.

ORCID

Kim Heybroek http://orcid.org/0000-0001-6452-2746

References

Achten, P.A.J., 2008. A serial hydraulic hybrid drive train for off-road vehicles. *Proceedings of the National Conference on Fluid Power*, 19 (2), 515–521.

Achten, P.A.J. and Palmberg, J.-O., 1999. What a difference a hole makes – the commercial value of the INNAS hydraulic transformer. *In*: *The 6th Scandinavian international conference on fluid power, SICFP'99*, 26–28 May. Tampere, Finland.

Andersson, S., Söderberg, A., and Björklund, S., 2007. Friction models for sliding dry, boundary and mixed lubricated contacts So. *Tribology International*, 40, 580–587. doi:10.1016/j.triboint.2005.11.014.

Belan, H.C., *et al.*, 2015. Digital secondary control architecture for aircraft application. *In*: *The seventh workshop on digital fluid power*. Austria: Linz, 21–39.

Bishop, E.D., 2007. *Digital hydraulic system*. US20070120662A1. US.

Bishop, E.D., 2009. Digital hydraulic transformer – approaching theoretical perfection in hydraulic drive efficiency. *In*: *The 11th Scandinavian international conference on fluid power, SICFP'09*. Linköping, USA.

Busquets, E. and Ivantysynova, M., 2015. Adaptive robust motion control of an excavator hydraulic hybrid swing drive. *SAE International Journal of Commercial Vehicles*, 8 (2), 2015-01–2853. doi:10.4271/2015-01-2853.

Dell' Amico, A. *et al.*, 2013. Investigation of a digital hydraulic actuation system on an excavator arm. *In*: *The 13th Scandinavian international conference on fluid power, SICFP2013*. Linköping, Sweden, 505–511. doi:10.3384/ecp1392a50.

Filla, R., 2015. Evaluating the efficiency of wheel loader bucket designs and bucket filling strategies with non-coupled DEM simulations and simple performance indicators. *Schriftenreihe der Forschungsvereinigung Bau- und Baustoffmaschinen e.V. FVB*, 49, 273–292. doi:10.13140/RG.2.1.1507.1201.

Frank, B., Skogh, L., and Alaküla, M., 2012. On wheel loader fuel efficiency difference due to operator behaviour distribution. *In*: *2nd commercial vehicle technology symposium (CVT 2012)*. Available from: http://www.iea.lth.se/publications/Papers/Frank_2012.pdf.

Hansen, A.H., 2014. *Investigation and optimisation of a discrete fluid power PTO-system for wave energy converters*. Aalborg, Denmark: Aalborg University, Institute of Energy Technology.

Hansen, R.H., Andersen, T.O., and Perdersen, H.C., 2011. 'Analysis of discrete pressure level systems for wave energy converters. *In*: *Proceedings of 2011 international conference on fluid power and mechatronics*. 552–558. doi:10.1109/FPM.2011.6045825.

Heemskerk, E., Bonefeld, R., and Buschmann, H., 2015. Control of a semi-binary hydraulic four-chamber cylinder. *In*: *Proceeding of the 14th Scandinavian international conference on fluid power*. Tampere, Finland.

Heybroek, K. and Norlin, E., 2015. Hydraulic multi-chamber cylinders in construction machinery. *In*: *Hydraulikdagarna*. Linköping, Sweden.

Heybroek, K., Vael, G.E.M., and Palmberg, J.-O., 2012. Towards resistance-free hydraulics in construction machinery. *In*: *8th international fluid power conference*. Dresden, Germany.

Huova, M., Laamanen, A., and Linjama, M., 2010. Energy efficiency of three-chamber cylinder with digital valve system. *International Journal of Fluid Power*, 11 (3), 15–22. doi:10.1080/14399776.2010.10781011.

Inderelst, M. *et al.*, 2011. Energy efficient system layout for work hydraulics of excavators. *In*: *The 12th Scandinavian international conference on fluid power, SICFP'11*. Tampere, Finland.

Linjama, M., *et al.*, 2009. Secondary controlled multi-chamber hydraulic cylinder. *In*: *Proceedings of the 11th Scandinavian international conference on fluid power, SICFP'09*. Sweden.

Palmgren, G. and Palmberg, J.-O., 1988. Secondary controlled hydraulic systems – A new drive concept with future prospects. *In*: *International fluid power exposition, IFPE'88*. Chicago, IL.

Pettersson, K. and Tikkanen, S., 2009. Secondary control in construction machinery – design and evaluation of an excavator swing drive. *In*: *The 11th Scandinavian international conference on fluid power, SICFP'09*. Linköping.

Sahlman, M., 2012. *Valve controlled multi-chamber cylinder*. Tampere: Tampere University of Technology.

Shih, M.-C., 1984. *Untersuchung einer zylinderansteuerung durch hydro-transformator am Konstant Drucknetz*. Aachen University.

Wiktor, R. and Heybroek, K., 2014. *Pressurized medium assembly*. US20150298730A1. Sweden.